Mechanosensitivity of N-Type Calcium Channel Currents

Barbara Calabrese,* Iustin V. Tabarean,* Peter Juranka,* and Catherine E. Morris*†
*Department of Neurosciences, Ottawa Health Research Institute, and †Department of Medicine, University of Ottawa, Ottawa, Ontario K1Y 4E9, Canada

ABSTRACT Mechanosensitivity in voltage-gated calcium channels could be an asset to calcium signaling in healthy cells or a liability during trauma. Recombinant N-type channels expressed in HEK cells revealed a spectrum of mechano-responses. When hydrostatic pressure inflated cells under whole-cell clamp, capacitance was unchanged, but peak current reversibly increased ~1.5-fold, correlating with inflation, not applied pressure. Additionally, stretch transiently increased the open-state inactivation rate, irreversibly increased the closed-state inactivation rate, and left-shifted inactivation without affecting the activation curve or rate. Irreversible mechano-responses proved to be mechanically accelerated components of run-down; they were not evident in cell-attached recordings where, however, reversible stretch-induced increases in peak current persisted. T-type channels (α_{1I} subunit only) were mechano-insensitive when expressed alone or when coexpressed with N-type channels (α_{1B} and two auxiliary subunits) and costimulated with stretch that augmented N-type current. Along with the cell-attached results, this differential effect indicates that N-type mechanosensitivity did not depend on the recording situation. The insensitivity of T-type currents to stretch suggested that N-type mechano-responses might arise from primary/auxiliary subunit interactions. However, in single-channel recordings, N-type currents exhibited reversible stretch-induced increases in NP_o whether the α_{1B} subunit was expressed alone or with auxiliary subunits. These findings set the stage for the molecular dissection of calcium current mechanosensitivity.

INTRODUCTION

Calcium influx through voltage-gated calcium channels is essential in many neuronal functions. The influx has immediate effects such as neurotransmitter release and the shaping of action potentials and firing patterns, plus long-term effects mediated via calcium-sensitive enzymes that regulate gene transcription, axonal outgrowth, neuronal migration, and more. Based on electrophysiological and pharmacological properties, different types of calcium channels (designated L-, N-, P-, Q-, R-, and T-type) have been distinguished (Moreno Davila, 1999; Catterall, 2000). Consistent with their central role in signal transduction, Ca^{2+} channels are heavily modulated.

Diverse unidentified, identified, and cloned channels from organisms as different as bacteria, plants, frogs, and rats exhibit mechanosensitive responses (Hamill and Martinac, 2001). The first evidence that calcium channels feel and respond to membrane stretch came from whole-cell voltage clamp of arterial myocytes (Langton, 1993), and evidence has subsequently accumulated that L-type currents in cardiac (Matsuda et al., 1996), gastric (Xu et al., 1996), arterial (Ruiz-Velasco et al., 1996; Kimura et al., 2000), and intestinal (Holm et al., 2000) smooth muscle and also pituitary cells (Matzner et al., 1996) and osteoblastic cells (Ryder and Duncan, 2001), increase with stretch and/or shear. However, the channels involved have been molecularly indeterminate, and morphologically diverse native cells have been used in conjunction with assorted mechanical stimuli (hydrostatic swelling, osmotic swelling, and extracellular perfusion) whose effects on cell geometry were not cross-correlated against the ongoing electrophysiological mechano-responses.

Here, we address calcium channel mechanosensitivity in a recombinant system. Expression of specific proteins, human brain N-type and rat brain T-type, in undifferentiated clonal cells (HEK cells) provided a standard cell morphology. Studying recombinant N-type was preferable to L-types because for N-type in HEK cells, inactivation is not mediated by the divalent charge carrier (Patil et al., 1998; Jones et al., 1999). During whole-cell recording, with inflation (positive pipette pressure) as the mechanostimulus, cell shape and pressure were continually monitored. Invariably, in cells that inflated, reversible and irreversible mechanosensitive changes occurred for the N-type currents. T-type currents made no response, a differential responsiveness that was surprising but was confirmed in cell-attached experiments.

MATERIALS AND METHODS

Constructs

Human embryonic kidney T-antigen-transformed (HEK-tsA201) cells were provided by G. Zamponi (University of Calgary, Calgary, AB). Human embryonic kidney (HEK 293) cells stably expressing the rat T-type Ca^{2+} channel (α_{1I}) were obtained from E. Perez-Reyes (University of Virginia, Charlottesville, VA). This version of the rat α_{1I} Ca^{2+} channel (GenBank accession number AF086827) used to generate this stable cell line is a C-terminally truncated version of the predicted full-length rat α_{1I} Ca^{2+} channel and appears to be missing a short section at the 3′ end of the coding sequence. This C-terminal truncation appears to have little functional effect on the electrophysiological properties of α_{1I} (Lee et al., 1999). Human brain cDNAs encoding α_{1B}, β_{1b}, α_2-δ subunits (N-type calcium

Submitted January 31, 2002, and accepted for publication July 3, 2002.

Address reprint requests to Dr. Catherine E. Morris, 725 Parkdale Avenue, Ottawa, Ontario K1Y 4K9, Canada. Tel.: 613-798-5555; Fax: 613-761-5330; E-mail: cmorris@ohri.ca.

0006-3495/02/11/2560/15 $2.00

channel) were obtained from M. W. McEnery (Case Western Reserve, Cleveland, OH). The cDNA for the enhanced green fluorescent protein was provided by G. Zamponi.

Cell culture and transient transfection

Cell lines (<20 passages) were maintained in Dulbecco's modified Eagle's medium (DMEM) with 10% fetal bovine serum and 1% penicillin/streptomycin at 37°C/5% CO_2. To sustain stable expression of rat α_{1I}, 1 mg/ml active geneticin (GIBCO-BRL, Burlington, Ontario, Canada) was added to the medium. Cells were grown to 80% confluency, split with 0.5 ml of trypsin-EDTA (1×) per 25-cm^2 flask, and plated at 10% confluency on 12-mm round glass coverslips. The next day, using a standard calcium phosphate protocol, we transiently transfected cells with cDNAs for human brain α_{1B}, β_{1b}, and α_2-δ subunits plus enhanced green fluorescent protein in a molar ratio of 3:3:3:2 (usually 6 μg/μl for each subunit, but for single-channel recordings from cells expressing all subunits, only 1 μg/μl/subunit). After 8–12 h, cells were washed with Dulbecco's modified Eagle's medium, allowed to recover for 12 h, and then incubated at 28°C for 1–3 days before recording. Products for cell line maintenance were obtained from GIBCO-BRL, and chemicals for recording solutions were purchased from Sigma Chemical Co. (St. Louis, MO).

Electrophysiology

Whole-cell and cell-attached patch clamp (Hamill et al., 1981) currents were recorded 36 h after transfection from isolated enhanced green fluorescent protein-expressing cells that were round or eye-shaped. Coverslips were attached to a chamber (Warner Instrument Corp., Hamden, CT) bottom with silicone grease. Recordings were obtained at room temperature (21–23°C) with an Axopatch-1D (Axon Instruments, Foster City, CA). Patch pipettes, made of borosilicate (N51A Garner, Claremont, CA; 1.15-mm inner and 1.65-mm outer diameter) had resistances of 1–3 MΩ when fire-polished for the whole-cell configuration. Electrode capacitance was compensated before disrupting the patch, with the amplifier's fast transient cancellation circuits. Series resistance was compensated up to 70% in all experiments except those designed for monitoring membrane area (see next section) and was routinely checked during the course of experiments. Currents were filtered at 1 kHz. Leak current was subtracted by a P/-4 protocol in the data acquisition software (pClamp6, Axon Instruments). Pipettes for cell-attached recording were coated with Sylgard (Sylgard 184, Dow Corning, Wiesbaden, Germany) and fire polished to achieve 4–5 MΩ with 100 mM $BaCl_2$ or higher in the case of single-channel recordings. Patches with low apparent channel density were chosen for experiments, but the brevity of unitary events prevented us from ascertaining N, the number of functional channels in any patch, with certainty. Pipette pressure was applied and monitored with a transducer (DPM-1B, Bio-Tek, Winooski, VT). Unchanging baseline currents during mechanostimulation indicated the cells did not exhibit endogenous mechanosensitive currents under our recording conditions. The presynaptic action potential (AP) recorded by Borst et al. (1995) was scanned, digitized, and scaled for use as a waveform for AP clamp recordings.

Membrane capacitance (C_m) and series resistance (R_a) measurements with and without cell inflation

To simultaneously monitor membrane area and ionic current, C_m, R_a, and I_{Ba} were obtained applying a double-voltage-step protocol (a 4-ms step from −90 to −70 mV, then a 240-ms step from −90 to +10 mV). We applied an off-line analysis method using the following equations from Pappone and Lee (1996): $R_a = \tau/C$ and $C_m = \Delta Q + I_{ss}\tau/V_p$. Capacitative charge was measured from the integral of the current transient (ΔQ). To correct for the exponential rise of the voltage step, all current I_{ss} was integrated and summed with a component equal to $I_{ss}\tau$. V_p is the amplitude of the applied voltage step (20 mV); I_{ss} is the current measured at steady state with respect to baseline before the step; and τ, the decay time constant of the capacitative transient, is calculated according to $I(t) = (I_o - I_{ss})\exp(-t/\tau) + I_{ss}$. We performed this analysis with a routine using Labtalk from Origin 6.0 (Microcal Software, Northampton, MA).

Solutions

Whole-cell recordings

The external recording solution contained (in mM) 20 $BaCl_2$, 1 $MgCl_2$, 10 HEPES, 40 tetraethylammonium (TEA)-Cl, 10 glucose, and 65 CsCl (pH 7.2 with CsOH; 315 mOsm) or, for activation and inactivation curves, closed-state inactivation, and double-pulse experiments (see Figs. 6, *A–D*, 8, and 9), 2 $BaCl_2$, 1 $MgCl_2$, 10 HEPES, 40 TEA-Cl, 10 glucose, and 105 CsCl (pH 7.2 with CsOH). The pipette solution contained (in mM) 105 CsCl, 25 TEA-Cl, 11 EGTA, 1 $CaCl_2$, and 10 HEPES (pH 7.2 with CsOH) unless otherwise noted. For low intracellular Cl^- conditions, the pipette solution contained (in mM) 120 *N*-methyl D-glucamine, 60 HEPES, 1 $MgCl_2$, and 10 EGTA (pH 7.3 with methanesulfonic acid), and an extracellular solution of 150 Tris, 1 $MgCl_2$, 10 $BaCl_2$ (pH 7.3 with methanesulfonic acid) was used. In some experiments ATP-Na_2 was added to the pipette solution or EGTA was replaced with BAPTA. Just before recording, coverslips were washed in a Tyrode's solution to avoid precipitation of $BaSO_4$ from streptomycin-SO_4 in the growth medium. Solution osmolarities were measured with a 3MO micro-osmometer (Advanced Instruments, Needham Heights, MA).

Cell-attached recordings

The composition of the bath solution, designed to zero the resting membrane potential was (in mM) 120 K-aspartate, 1 $MgCl_2$, 5 EGTA, 10 HEPES, and 20 KCl (pH 7.4 with KOH; 320 mOsm with sucrose). Patch pipettes were filled with a solution of the following composition (in mM): 100 $BaCl_2$, 10 TEA-Cl, and 10 HEPES (pH 7.4 with TEA-OH).

Single-channel recordings

High-resistance pipettes (10–16 MΩ with 100 mM $BaCl_2$) were used, and seals usually exceeded 30 GΩ. Leak and capacitive current subtraction was performed by averaging segments of traces with no activity from the same voltage protocol in the same experiment and subtracting this average from each episode using pClamp 8.1 (Axon Instruments). Currents were recorded with an Axopatch 200B, sampled every 100 μs, filtered online at 2 kHz, and then off-line Gaussian filtered at 1 kHz. Openings to main and subconductance levels were observed in all patches (as is evident in the all-points histograms in Figs. 11 and 12) but were not analyzed separately. Single-channel activity (formally, the sum for each unitary current level, i, of iNP_o where N is the number of functional channels and P_o the probability of being open) was obtained from the all-points histograms by fitting with the pClamp 8.1 routine for weighted sum of Gaussians for open states.

Analysis of electrophysiological data

Graphs and curve fittings were done with Origin 6.0. The peak I/V relationships were fitted to the following transform of a Boltzmann function:

$$I = G_{max}(V - V_{rev})/\{1 + \exp[-(V - V_{0.5})/k]\},$$

where I is the peak I_{Ba} elicited by V, the test voltage, V_{rev} is the reversal potential, G_{max} the maximal conductance, $V_{0.5}$ the voltage for half-maximal

activation, and k the slope factor (in millivolts). The inactivation and activation curves were fitted by the Boltzmann function:

$$I/I_{max} = 1/\{1 + \exp[V_{0.5} - V)/k]\},$$

with k made negative in the case of inactivation and $V_{0.5}$ applied to half-maximal activation or inactivation as appropriate. Because run-down of I_{Ba} did not follow a simple exponential time course, it was quantified as the time to decline to 50% of the maximum I_{peak} after whole-cell access ($t_{1/2}$).

Cell volume measurements

Imaging of cells was via the inverted microscope's (Hoffman modulation, ×40, NA 0.5 objective) CCD camera (Hitachi Denshi Canada, Ltd., Nepeah, ON) whose video output was fed into a JVC time-lapse VCR for off-line analysis using a frame grabber DT3155 (Data Translation, Marlboro, MA). Images were collected during electrophysiological recording and collated by synchronization of pClamp and time-lapse VCR timers. The cross-sectional area (CSA) of traced regions was determined with ImageJ 1.06 (NIH Image), and cell borders were traced on the monitor by mouse and computer-generated cursor. Each image was traced twice, and the values were averaged. This analysis process allowed detection of changes in cell CSA with an accuracy of 2–3%. We calculated relative cell volume changes (Vol/Vol_0) using the equation Vol/Vol_0 = ((test CSA)/(control CSA))$^{3/2}$ (Churchwell et al., 1996).

Statistics

Results are presented as means ± SE. Except where noted, comparison was by unpaired or paired t-test, used as appropriate. Significance level was $p < 0.05$.

RESULTS

Ba^{2+} current just after whole-cell access: run-up and run-down

Human neuronal α_{1B}, β_{1b}, and α_2-δ subunits were transiently expressed in HEK 293-tsA201 cells. To avoid confounding stretch- and time-dependent effects in our experimental conditions, currents were first characterized over time. After obtaining the whole-cell configuration, cells were clamped to −90 mV and Ba^{2+} current (I_{Ba}) was elicited by a 240-ms step to +10 mV (Fig. 1 *A*). During the first 5–30 s after whole-cell access, a spontaneous increase in peak I_{Ba} (i.e., run-up) was observed, followed by a slower decline (i.e., run-down; Fig. 1, *A* and *B*). During the post-access period, there was an increase in the activation rate (Fig. 1 *A*, *inset*). Run-down was significantly slower (e.g., Fig. 2 *A*) for an inter-episode interval of 15 s than for 5 s ($p < 0.001$; $n = 6$), indicating that N-type Ba^{2+} current run-down was caused, at least in part, by cumulative inactivation.

Simultaneously we monitored, over time, the speed of inactivation (Fig. 1 *B*). Just after whole-cell access, inactivation was sufficiently slow that even with pulse durations of hundreds of milliseconds, fits to exponentials were unreliable; as an arbitrary index of inactivation speed, therefore, we calculated the extent of inactivation during a 240-ms pulse (e.g., Fig. 1 *B*, *right-hand axis*). As Fig. 1, *A* and *B* (*right axis*) indicates, inactivation speeded up until it reached a plateau (Fig. 2 *B*).

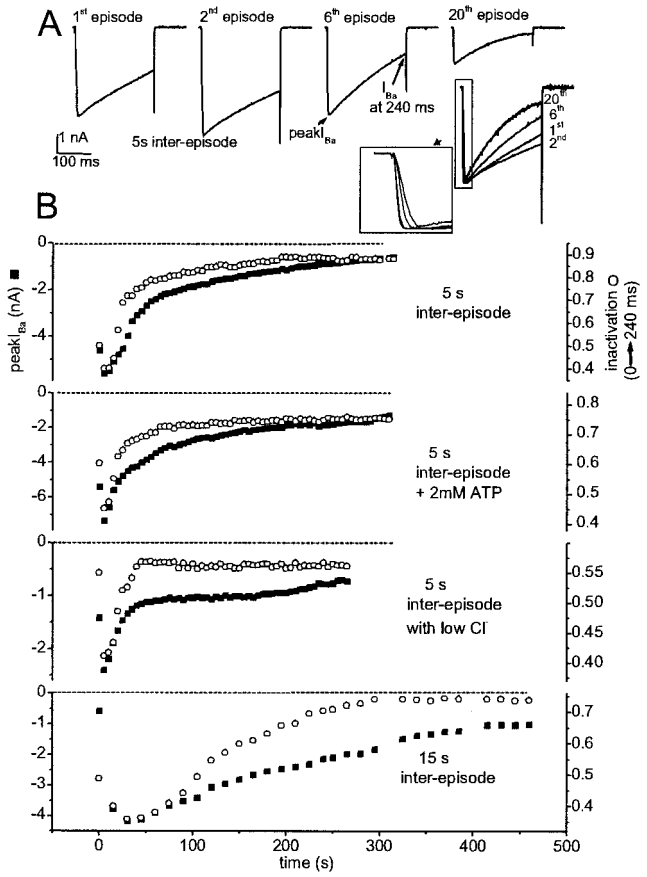

FIGURE 1 After whole-cell access, I_{Ba} shows run-up followed by run-down. (*A*) Selected whole-cell current traces elicited by a 240-ms test pulse (from −90 to +10 mV) from the 5-s inter-episode experiment of *B*. On the right, normalized versions of these traces are plotted to emphasize kinetic changes; the expanded boxed area (*arrow*; box width, 30 ms) demonstrates that it was possible to resolve a post-access increase in activation rates. (*B*) Peak I_{Ba} (■) and I_{Ba} inactivation (○) during a 240-ms test pulse (inactivation 0→240 ms quantified as $1 - (I_{240ms}/I_{peak})$) plotted versus time, from representative cells of four experimental conditions differing in inter-episode intervals (5 and 15 s) and intracellular solution.

Unlike run-down, run-up of peak I_{Ba} coincided with a slowing of inactivation; i.e., during the run-up period, the inactivation index fell (Fig. 1 *B*). This suggested that current contained a slowly recovering component, a possibility tested by pulsing at several higher frequencies (0.2-, 0.3-, and 0.4-s inter-episode intervals). Because an initial run-up of peak I_{Ba} was absent at these higher frequencies (Fig. 2 *C*; the absolute value of I/I_{max} falls continuously), we suspect that frequent pulsing prevented slow-mode channels from recovering from inactivation. This would also be consistent with the finding (data not shown) that during frequent pulsing as in Fig. 2 *C*, inactivation speed was constant.

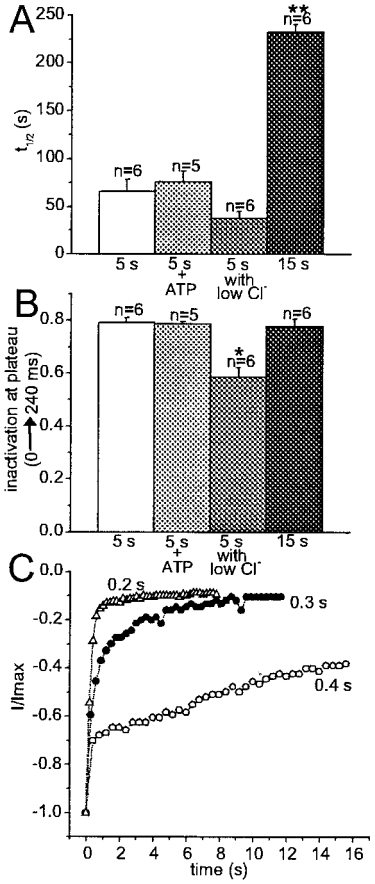

FIGURE 2 Run-down is reduced by long inter-episode intervals, whereas run-up does not occur during frequent pulsing. (*A*) For different combinations of inter-episode intervals and intracellular solution, times to decline to 50% of the maximum I_{Ba} after whole-cell access ($t_{1/2}$) were averaged (**$p < 0.001$, multiple comparison Tukey test of the three 5-s inter-episode conditions compared against the 15-s inter-episode condition; n = number of cells). (*B*) Levels at which inactivation stabilizes with different inter-episode intervals, adding ATP or reducing the concentration of Cl^- (*$p < 0.001$, multiple comparison Tukey test of 5-s inter-episode condition with low Cl^- versus all the other conditions; n = number of cells per bar). (*C*) Peak values of inward I_{Ba} at +10 mV were normalized and plotted versus time at different inter-episode intervals (0.4, 0.3, and 0.2 s) for three representative cells (different symbols for each).

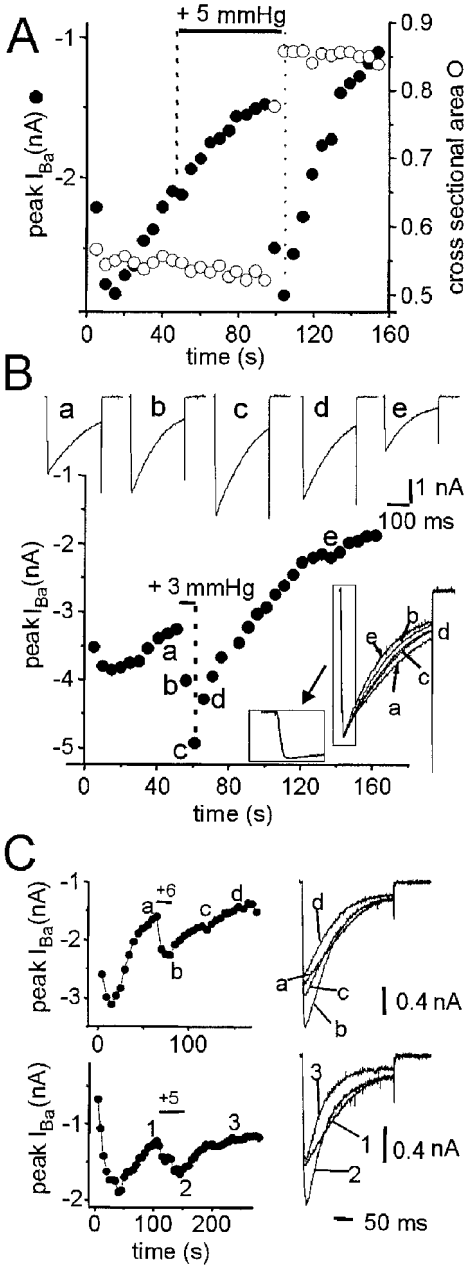

FIGURE 3 I_{Ba} peak increases with membrane stretch. (*A*) Peak $I_{Ba}(t)$ (●) for a representative cell, elicited at 5-s intervals, by steps from −90 to +10 mV. Pressure (mm Hg) was applied until an obvious volume change occurred. Cross-sectional area (○) is expressed $\times 10^3$ μm^2. (*B*) Peak $I_{Ba}(t)$ for a cell that inflated immediately upon application of pressure. Selected current traces (*a–e*) from the time course below are normalized in the lower right inset, the boxed part of which is expanded (*arrow*; box width, 30 ms), showing that the activation rate was unaffected by stretch. From *a* to *c*, increasing I_{Ba} represents the effect of positive pressure. At *d* (stretch off), the effect had begun to reverse. (*C*) Peak $I_{Ba}(t)$ for two representative cells elicited at 5-s intervals by steps from −90 to 10 mV, using 10 mM Ba^{2+} and 11 mM EGTA in the pipette. Selected current traces (*a–d*; 1–3) are shown from these time courses.

Use of more physiological pipette solutions (with ATP or low Cl^-) did not significantly alter the time course of run-down (Figs. 1 *B* and 2 *A*) or run-up (Fig. 1 *B*). Despite significantly slower run-down with 15-s inter-episode intervals, we mostly used the 5-s protocol; 15-s intervals proved impractical for monitoring rapid responses to membrane stretch (Fig. 3 *A*). For all solutions, the tendency for inactivation to speed up over time was evident, although for low Cl^- (e.g., Fig. 1 *B*, *right axis*), this reached a plateau at a significantly smaller value ($p < 0.001$, multiple comparison Tukey test versus 5 s; Fig. 2 *B*).

If free Ba^{2+}accumulated and caused run-down, then the percent run-down should correlate strongly with the maximal run-up I_{Ba} magnitude in any cell, an effect that would intensify with longer barium influx. Instead, for $n = 12$ cells

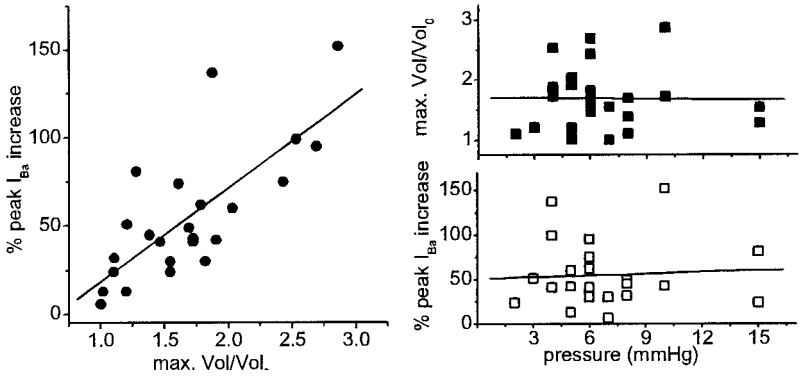

FIGURE 4 The mechanical stimulus in the whole-cell configuration. (*Left*) Inflation-induced current increase versus the maximal inflated volume ($n = 24$, $R = 0.75$). (*Right*) Neither maximal inflated volume nor inflation-induced I_{Ba} increase correlated with the applied pressure ($n = 24$, $R = -0.012$; $n = 24$, $R = 0.05$).

(maximal I_{Ba} range, -2 to -9.5 nA), when percent run-down after 10 and then 20 depolarization episodes was plotted (not shown) against maximal I_{Ba}, the correlation was weak, with regression coefficients of -0.4 and then -0.3 ($+0.4$ and $+0.3$ for I_{Ba} taken as positive).

Effect of membrane stretch on the amplitude of peak I_{Ba}

Cell volume was manipulated via pressure in the recording pipette and was monitored by video-microscopy. Whenever positive pressure succeeded in producing a volume increase (e.g., Fig. 3 *A*), this was accompanied by a current increase. Although visible inflation often lagged behind the onset of pressure, they coincided in Fig. 3 *B* (CSA not shown). Enhancement of peak currents coinciding with inflation was also observed for experiments using BAPTA (not shown). If the mechanically induced increase in peak I_{Ba} were an artifact of increased divalent buffering during inflation (resulting from blowing in EGTA), then pipette solutions that either clamp buffer capacity or slightly increase cytoplasmic [Ba^{2+}] during inflation should eliminate the stretch effect. In a series of tests, therefore, we added Ba^{2+} to the pipette so that solution blown into the cell would have a known low level of free Ba^{2+}. Specifically, we inflated cells using a 0.3 mM free Ba^{2+} solution (calculated with MaxChelator freeware for the regular 11 mM EGTA pipette solution except with 10 mM Ba^{2+} used instead of 1 mM Ca^{2+}). As seen in Fig. 3 *C*, inflating with this solution did not discernibly alter the outcome. The run-down time (70 ± 26 s; $n = 4$ cells) was not significantly different and, critically, the response to inflation was like that for the control pipette solution: peak I_{Ba} increased 1.5-fold $\pm$ 0.1($n = 4$), and inactivation speeded up with stretch. These data strongly suggest that the inflation effect was not mediated chemically but was mediated mechanically by membrane stretch.

We, like Langton (1993), sometimes found that substantial pressures ($+30$ and $+50$ mm Hg) would not yield a perceptible change in cell volume. In those cases, there was no increase in I_{Ba}. Partially blocked pipette tips may have prevented such cells from experiencing the applied pressure even though access for voltage clamp was adequate. Confirming that inflation was the critical parameter, peak I_{Ba} increase correlated strongly with the cell volume change (Fig. 4, *left*) but was uncorrelated with the magnitude of pressure applied (Fig. 4, *lower right*). Another plot (Fig. 4, *upper right*) demonstrates that maximum inflation was not a function of pressure.

To ascertain whether shifting *I*/*V* relations explained the peak effect, we recorded I_{Ba} with 20 mM Ba^{2+} in the bath before, during, and after inflation (not shown). Although the fitted G_{max} increased significantly from 18 ± 2 nS to 26 ± 2 nS, equivalent to recruiting 800 units of 10 pS via inflation ($p < 0.005$, paired *t*-test; $n = 6$), peak I_{Ba} scaled up to the same extent across all voltages (e.g., at -10 mV and $+30$ mV, I_{during}/I_{before} was 1.5 ± 0.1 and 1.5 ± 0.2, respectively) and the reversal potential (54 ± 1 mV before and 55 ± 2 mV during and after) was unaffected. In other words, there was no evidence for an inflation-induced shift in the *I*/*V* relations.

R_a and C_m during applied pressure

To determine whether inflation-induced increases of I_{Ba} required an increased membrane area, membrane capacitance (C_m), $I_{Ba,}$ and CSA were measured simultaneously with and without pressure. To preserve the capacitative transients needed for determining C_m and R_a (see Materials and Methods), leakage current was not subtracted on-line. A raw current trace sequence in Fig. 5 (*top*) illustrates that stretch increased peak I_{Ba} with no change in leakage current (unchanged baseline). Note that although stretch increased both peak I_{Ba} and CSA, C_m decreased and did not change more than 2%. For five stretch measurements with positive pressures ($n = 4$ cells) the average absolute percent change in C_m ([maximal ΔC_m during stretch]/[mean C_m prestretch] $\times$ 100) was 2.8 ± 0.6%, with increases in two of five and decreases in three of five measurements. During the entire illustrated experiment, series (i.e., access) resistance (R_a) (Fig. 5, *center*) varied <5% (the change for $n = 5$ was 4.6 ± 0.6%; 3 decreased, 1 increased, and 1 unchanged).

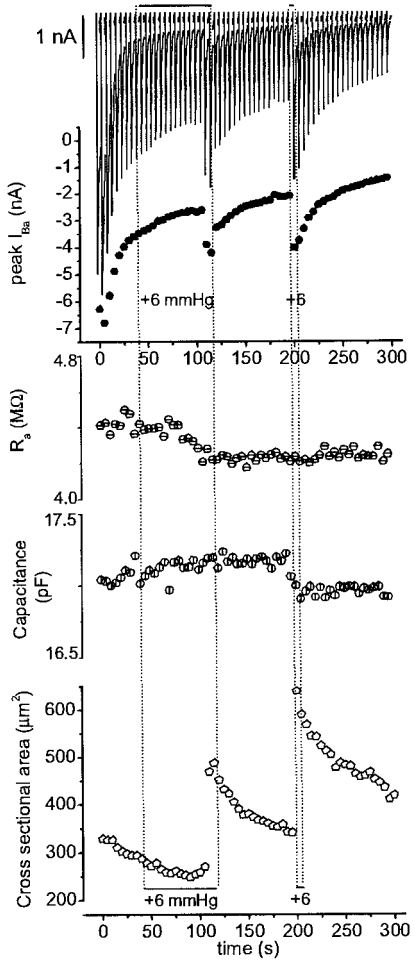

FIGURE 5 Simultaneous changes in I_{Ba}, R_a, C_m, and CSA before, during, and after pressure in a representative cell. (*Top*) Raw current traces (no leak subtraction) elicited by 240-ms pulses from −90 mV to +10 mV at 5-s intervals and the corresponding I_{Ba} peaks plotted versus time. (*Center*) Series resistance (R_a) and membrane capacitance (C_m) calculated from 4-ms prepulses (see Materials and Methods) and plotted versus time. (*Bottom*) CSA measurements versus time.

Effect of stretch on inactivation and activation curves

A double-pulse protocol was used to generate inactivation curves for I_{Ba} (Fig. 6, *A–C*). Prepulse potentials (−130 to +10 mV) were applied for 7 s, and then after a 10-ms interval, at −100 mV, the membrane was stepped to +10 mV for 240 ms (i.e., test pulse). The recovery time allowed between 7-s prepulses was 10 s. Test currents, normalized to those obtained for the −130-mV prepulse, were plotted against prepulse potentials and fitted by a Boltzmann equation (see Materials and Methods). Time control recordings (over 4–16 min; $n = 10$) showed a spontaneous 7-mV leftward shift (Fig. 6 *A*) with initial and final half-inactivation voltages ($V_{0.5}$) at −73 ± 0.9 mV and −80 ± 0.7 mV and no change in slope factor (k; 12 ± 0.8 mV versus 12 ± 0.7 mV). For cells maintained in an inflated condition by positive pressure over a 4–19-min interval ($n = 12$; Fig. 6 *B*), an 18-mV leftward shift was obtained ($V_{0.5} = -73 \pm 0.9$ mV without stretch and −91 ± 0.9 mV with stretch), with k constant at 13 ± 0.8 mV before and during stretch. The stretch-induced $V_{0.5}$ shift, which developed gradually and was irreversible (Fig. 6 *C*), was significantly larger than the spontaneous shift ($p < 0.0009$, unpaired t-test).

Activation data in time control (not shown) and stretch experiments (Fig. 6 *D*) were fitted with a Boltzmann equation (see Materials and Methods). The curves were obtained by stepping in 10-mV increments from $V_h = -100$ mV to +70 mV, starting from −70 mV, for 20 ms before repolarizing to −50 mV. Activation $V_{0.5}$ values and k (in mV) showed no significant changes with time (from $V_{0.5} = -1.9 \pm 0.6$ and $k = 7.4 \pm 0.5$ to $V_{0.5} = -2.3 \pm 0.6$ and $k = 7.9 \pm 0.5$, 4–8 min later; $n = 5$) or with stretch (from $V_{0.5} = -1.7 \pm 0.7$ and $k = 8.5 \pm 0.7$ for the control to $V_{0.5} = -2 \pm 0.5$ and $k = 8.7 \pm 0.5$ with stretch over 4–10 min; $n = 7$).

Kinetic properties of I_{Ba} during stretch

The rate of activation of I_{Ba} with and without stretch was compared for normalized current peaks (e.g., Fig. 3 *B*, *inset*, and Fig. 7 *B* for steps from −90 mV to +10 mV). In all cells tested, and over a wide range of voltages, no effect of stretch on the activation rate was observed. Stretch did not, therefore, increase peak I_{Ba} via this mechanism.

The gradual speeding of open-state inactivation invariably seen in 5-s inter-episode recordings (e.g., Fig. 1 *B*) was immediately accelerated by stretch, as Fig. 7, *A* and *B*, illustrates. Stretch acceleration of open-state inactivation was transient rather than irreversible (e.g., Fig. 7 *A*, +4 mmHg). Additionally, although it was dramatic early in the recordings, stretch acceleration could not be elicited at all once inactivation speed reached a plateau (e.g., Fig. 7 *A*). This changing effectiveness of stretch is summarized quantitatively in Fig. 7 *C*.

N-type channels inactivate preferentially from intermediate closed states (Patil et al., 1998), so we tested whether stretch affected this process using a protocol involving 20-pulse trains (10-ms pulses, from −90 to +10 mV, with a 50-ms inter-episode; Fig. 8 *A*). The extent of closed-state inactivation over the course of these trains was quantified as the proportion: 1 − (last pulse current/first pulse current). As illustrated in Fig. 8 *C* (*left*), membrane stretch (+7, +4, and +7 mmHg) dramatically enhanced the process of inactivation from intermediate closed states. On the right side of Fig. 8 *C*, the graph for selected 20-pulse trains (*a–e*) from this cell illustrates in fuller detail that stretch acted in a progressive and irreversible manner. Fig. 8 *B*, which charts the process over time (100, 200, 300, and 400 s) in control cells versus cells subjected to stretch, indicates that stretch augmented a background time-de-

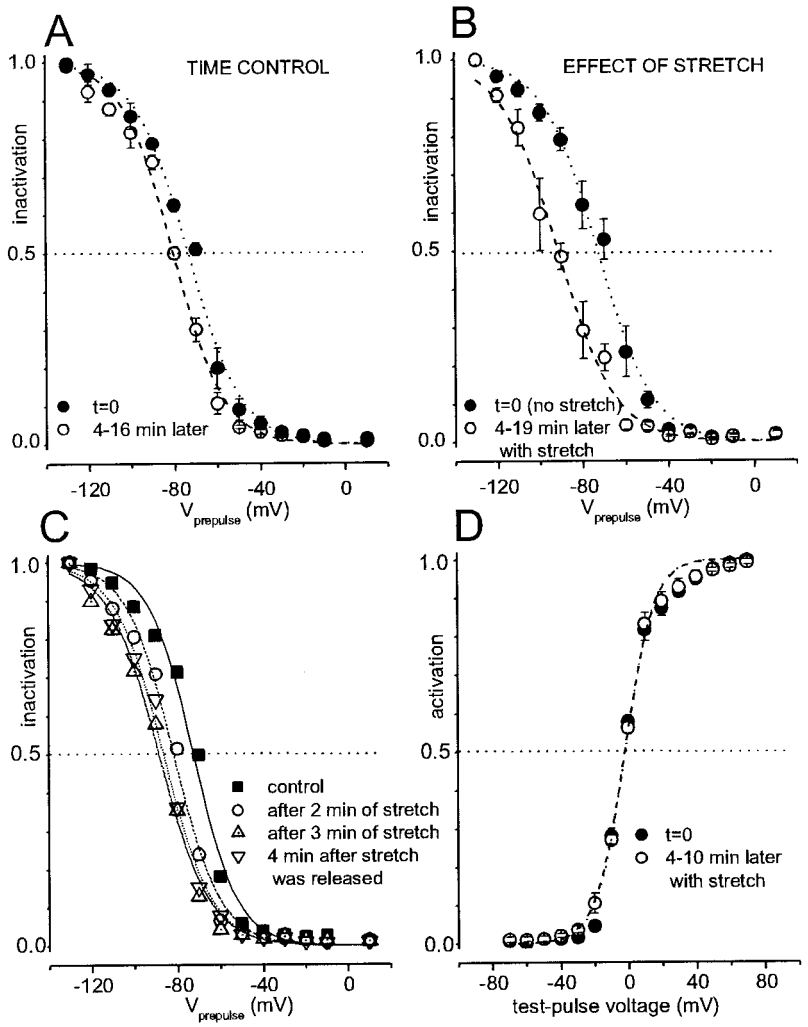

FIGURE 6 Activation and inactivation curves with and without stretch. (*A*) Inactivation relationships (n = 10), obtained just after whole-cell access (●) and after a 4–16-min interval (○): ●, $V_{0.5} = -73 \pm 0.9$ mV and $k = 12 \pm 0.8$ mV; ○, $V_{0.5} = -80 \pm 0.7$ and $k = 12 \pm 0.7$ mV. Currents with 2 mM Ba^{2+} normalized to current obtained with −130-mV prepulse (inactivation = I/I_{max}) and fitted by the inactivation Boltzmann (see Materials and Methods). (*B*) Inactivation relationships (n = 12) with no stretch just after access (●) and after 4–19 min with stretch (○): ●, $V_{0.5} = -73 \pm 0.9$ mV and $k = 13 \pm 0.8$ mV; ○, $V_{0.5} = -91 \pm 0.9$ mV and $k = 13 \pm 0.8$ mV. The $V_{0.5}$ shift with stretch was significantly larger ($p < 0.0009$, unpaired t-test). (*C*) Inactivation curves from a single cell. (*D*) Steady-state activation curves (n = 7) with no stretch just after access (●) and after 4–10 min with stretch (○): ●, $V_{0.5} = -1.7 \pm 0.7$ mV and $k = 8.5 \pm 0.7$; ○, $V_{0.5} = -2 \pm 0.5$ amd $k = 8.7 \pm 0.5$ mV. Data were fitted by the activation Boltzmann (see Materials and Methods).

pendent increment in the speed of inactivation from intermediate closed states. Not surprisingly, 10-ms depolarizing steps separated by 980 ms (corresponding to first and last pulses only in the 20-pulse trains) elicited identical currents (Fig. 8 *D*, *left*), as expected if, during the earliest 20-pulse trains, inactivation occurred preferentially from intermediate closed states. That said, over time (50−450 s was tested; Fig. 8 *D*, *right*), the relative height of I_{Ba} at the end pulse did diminish. This loss (i.e., during the uninterrupted 980-ms interval at −90 mV) was significantly ($p < 0.005$, Wilcoxon signed rank test) enhanced by membrane stretch. Simultaneously, a minor time-dependent increase (e.g., see *arrows* in Fig. 8 *D*, *left*) in the activation rate was measured ($\tau = 2.2 \pm 0.5$ ms at $t = 0$ s and 1.5 ± 0.4 ms at $t = 400$ s; $n = 6$; $p < 0.006$, paired t-test), but this was unaffected by stretch. Yet again, therefore, we found that even as stretch was enhancing a spontaneously occurring (i.e., time-in-whole-cell-configuration-dependent) process, it had no impact on activation kinetics.

Differential stretch effects on T- and N-type I_{Ba}

Whole-cell recordings

In the next series of experiments we asked 1) whether low-voltage-activated calcium channel currents (T-type) were mechanosensitive like the high-voltage-activated N-type and L-type channel currents and 2) whether T- and N-channels in the same cellular setting responded in a channel-specific manner to stretch. Whole-cell recordings were made with a double-pulse protocol that activated both types of currents but also allowed them to be dissected. For the first question we used HEK cells stably transfected with the α_{1I} (T-type calcium channel) subunit, and for the second question we transiently transfected into this cell line the human α_{1B} (N-type calcium channel), β_{1b}, and α_2-δ subunits. As demonstrated in Fig. 9 *A*, in cells stably expressing T-type channels only, −30 mV and +10 mV elicited large and small inward currents, respectively. Stretch had no discernible impact on these T-type currents at either voltage; increasing the inflationary pressure until rupture did not change this (n = 3). By contrast, when only N-type

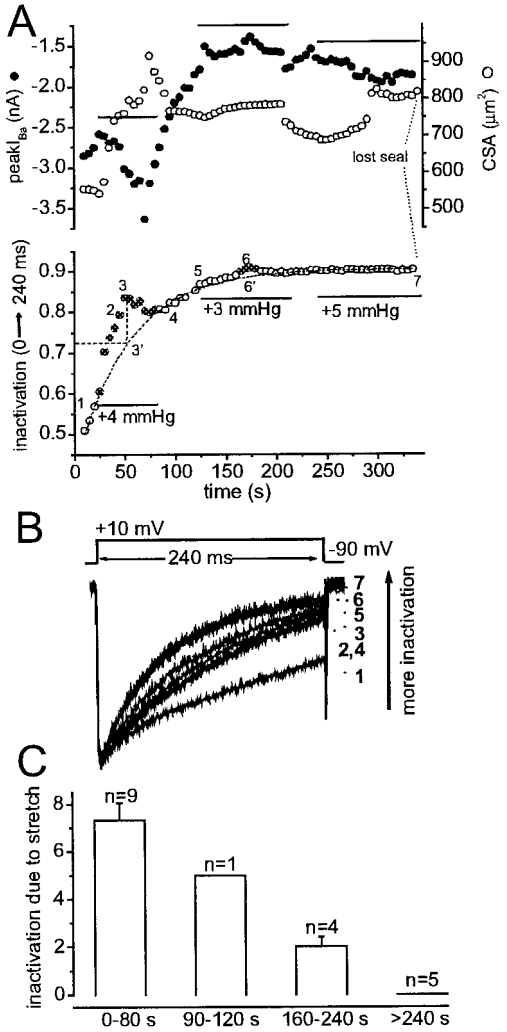

FIGURE 7 Membrane stretch and the rate of open-state inactivation. (*A*) Time course of peak I_{Ba} and, below this, of inactivation rate, in a representative cell. Bars indicate positive pressure applied to the pipette (note the abrupt early increase in volume or CSA). A first-order exponential fit (*dashed line*) including only data corresponding to the white dots, avoiding the nonlinear region of the hatched dots, corresponds to the time course for inactivation rate expected in the absence of stretch. Primed numbers on this line thus represent expected-without-stretch values. (*B*) Normalized current traces from the above time course, as numbered. (*C*) For experiments like that illustrated in *A*, the bar graph summarizes over time the diminishing effect of stretch on inactivation speed (stretch effect given as percent difference between the value observed with stretch and the interpolated exponential no-stretch value).

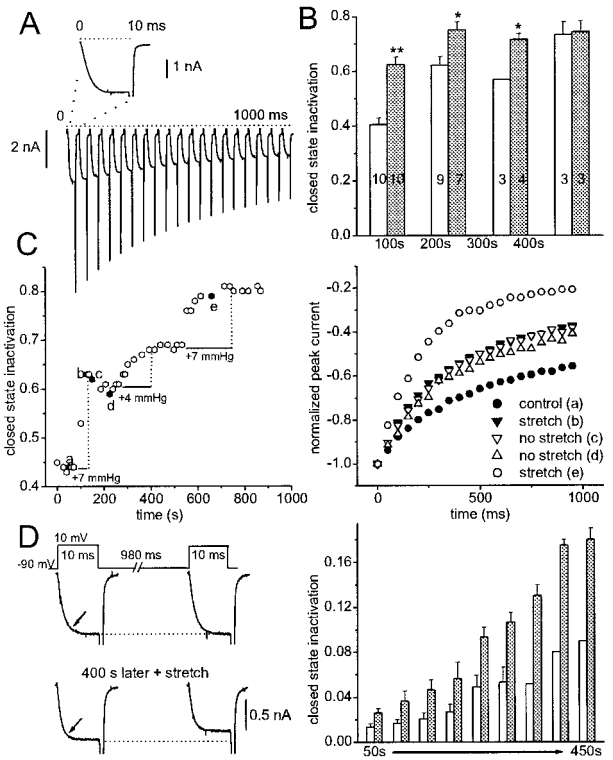

FIGURE 8 Membrane stretch and closed-state inactivation. (*A*) Representative currents elicited by a 1-s train of 20 pulses of 10 ms (hence, 50-ms inter-episodes). The expanded current trace shows no apparent inactivation from the open state. (*B*) From experiments as illustrated in *C*, average values for inactivation from closed states were calculated every 100 s after recording began, either in cells that were not stretched (*white bars*) or those under stretch when the measurement was obtained (*gray bars*). Number of cells is given in the bars (**$p < 0.00001$; *$p < 0.01$ (200 s); *$p < 0.002$ (300 s); $p < 0.9$ (400 s)). The extent of inactivation at the indicated times was quantified as the decimal fraction $1 - (I_{\text{peak, 20th pulse}}/I_{\text{peak, 1st pulse}})$. (*C*) For a sample cell, inactivation from intermediate closed states plotted versus time (*left*) with normalized peak currents (*right*) with and without stretch from selected times (different symbols; locate *a–e* at *left*). (*D*) On the left are representative currents elicited by a 1-s train of two pulses (10 ms) 980 ms apart (i.e., first and last pulses only of the train used for *A–C*), taken at the beginning of an experiment (*top*) and 400 s later during stretch (*bottom*). On the right is shown the extent (decimal fraction) of inactivation from deep closed states, calculated at 50-s intervals after the start of recording in three no-stretch control cells (*white bars*) and three cells for which stretch was present during the measurements (*gray bars*); *n* values for control:stretch are thus 3:3 (*white*:*gray*), except for late times (350, 400, and 450 s) when loss of seals reduced *n* values to 1:2.

channels were expressed (Fig. 9 *B*), −30 mV elicited no current and +10 mV elicited large inward currents, and as we have now come to expect, stretch increased the current at +10 mV. Next the two channels were coexpressed so they could simultaneously be subjected to precisely the same mechanical stimulus. As illustrated in Fig. 9 *C*, stretch did not affect the current elicited at −30 mV (this is T-only current) yet increased that at +10 mV ($n = 5$). Taken together with the control for T-type (as in Fig. 9 *A*), we conclude that the entire effect at +10 mV was caused by an N-type current response to stretch. This amounted to 1.4 ± 0.1-fold peak increase ($n = 7$). Notice that the imposed cell inflation did not affect the baseline between steps or during steps when no voltage-dependent current was elicited (e.g., Fig. 9 *B*, −30 mV).

Cell-attached recordings

Because the cell-attached patch recording preserves the content of the cytoplasm and provides a different way

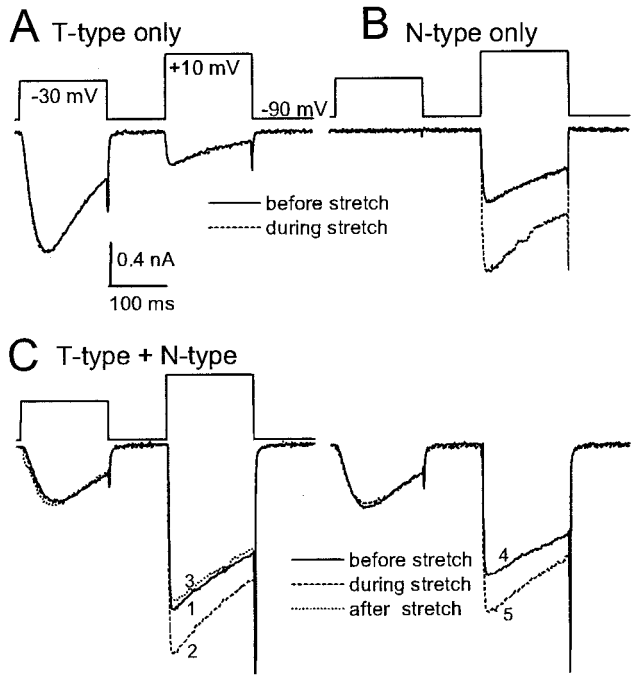

FIGURE 9 Differential stretch effects on whole-cell T- and N-type I_{Ba}. The double-pulse protocol was applied to a cell transfected with only T-type calcium channels (*A*) and a cell transfected with only N-type calcium channels (*B*). (*C*) Double-pulse protocol activates T-type (−30 mV) and N-type (+10 mV) currents in the same cell. Numbers 1–5 indicate the sequence of the raw traces with an interval of 5 s between 1, 2, and 3 and 4 and 5 and 15 s between 3 and 4. Solid, dashed, and dotted lines indicate the presence or absence of positive pressure during the recording. The repeated application of positive pressure (+9 mm Hg during trace 2; +5 mm Hg during trace 5) elicited 1.3- and 1.2-fold peak increases of the N-type current whereas the T-type current did not change. Bath solution contained 2 mM Ba^{2+}.

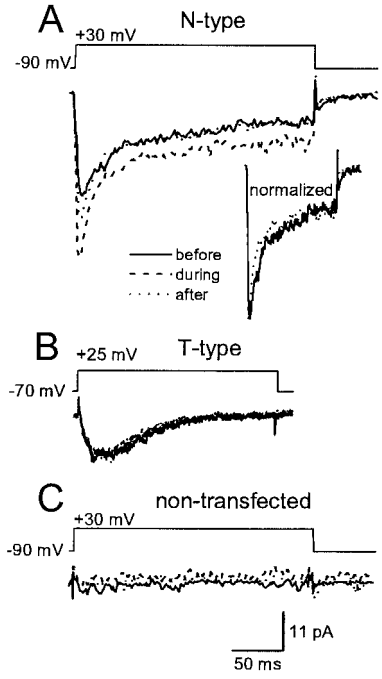

FIGURE 10 Differential stretch effects on T- and N-type I_{Ba} from cell-attached patches. (*A*) Representative N-type currents elicited by a 240-ms pulse showing a 1.6-fold increase during membrane stretch. The inset shows the same traces normalized. (*B*) Representative T-type currents before, during, and after stretch. (*C*) Representative traces recorded from a nontransfected cell before, during, and after stretch. To help reveal the traces with and without stretch, traces were Gaussian filtered at 500 Hz. Scale bars are the same for all the traces.

(pipette aspiration) to subject membrane to tension, we performed some experiments in this configuration. To obtain macroscopic N-type or T-type currents from the patches, pipettes of ~2-μm inside diameter (after polishing) were used. At the beginning of recordings of N-type current (one pulse every 5 s), run-up was evident (data not shown), but the currents stabilized by ~25 s, and thereafter there was no evidence of run-down. Every time suction in the range of −15 to −55 mmHg was applied to patches to generate membrane stretch, a reversible increase in the peak (and sustained) N-type current was observed (Fig. 10 *A*). The increase averaged 33 ± 6% (n = 9, from six patches) or 1.3-fold. In five of six patches, inactivation was unaffected by stretch, although in a sixth (Fig. 10 *A*, *inset*) it showed a minor change. For patches from cells expressing T-type current (Fig. 10 *B*), no change was observed when pressure was applied (n = 6) and then, with successive pulses, increased until rupture occurred. Likewise, stretch did not elicit currents in nontransfected cells (n = 3; Fig. 10 *C*).

Single-channel recording

In our macroscopic recordings, stretch reversibly increased N-type I_{Ba} without detectably accelerating its onset. One possible explanation was that stretch increased unitary current. To examine this, we made cell-attached single-channel recordings of N-type I_{Ba}, both for channels in cells expressing the α_{1B} subunit alone (see Meir and Dolphin, 1998) and for cells coexpressing the α_{1B}/α_2-δ/β_{1b} combination (for the latter, the quantities of cDNAs were reduced). The small membrane patches used in these experiments would necessarily have encompassed less long-range structure than large patches used for macroscopic recording. Consequently, the single-channel recordings represent the simplest situation (mechanically speaking) in which we tested effects of stretch on N-type channels. To collect enough events for even the simplest analyses, stretch was applied continuously during and between depolarizing steps, so even though the patches were initially formed as gentle patches (as defined by Small and Morris, 1994), the data were collected from nongentle patches.

Single-channel data with and without stretch are seen in Figs. 11 (α_{1B} subunit alone) and 12 (the α_{1B}/α_2-δ/β_{1b} combination). Raw data from several patches are included, illustrating the range of prestretch channel activity in our

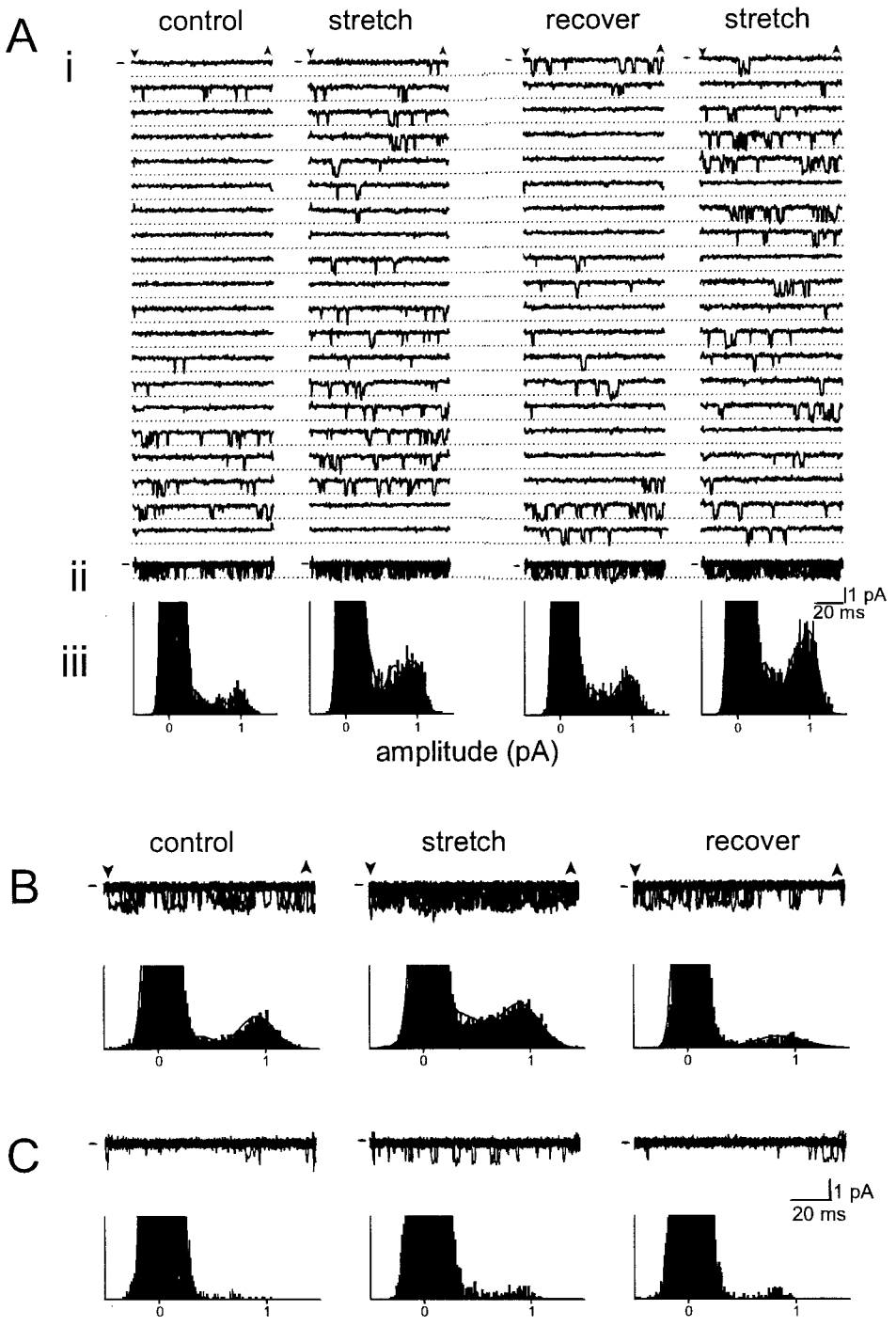

FIGURE 11 Patch stretch increases NP_o when α_{1B} is expressed alone. (*A*) Consecutive current responses elicited by 100-ms voltage steps to 20 mV from a V_h of −70mV every 6 s (*i*), the same 20 episodes shown overlapped (*ii*), and the all-points amplitude histograms of these traces (*iii*; bin-width, 0.014 pA). Keeping the histogram ordinate scale fixed, the closed level (baseline) peaks were truncated to emphasize the open levels. Down/up arrowheads indicate the beginning and end of test depolarizations. Faint dotted lines correspond to 1 pA from baseline. (*B* and *C*) Twenty overlapped consecutive traces and all-points histograms for two other patches, before, during, and after stretch.

patches. For the entire collection of patches tested before, during, and after stretch (at one or more suction levels), Fig. 12 *B* plots the single-channel activity (means and errors) obtained from analysis of the all-points histograms. Because the high-concentration divalent pipette solutions (100 mM Ba^{2+} was used) needed for single-channel recording right-shift the *I*/*V*, 20 mV was used as the test voltage. Within-patch comparisons of these data sets showed that stretch significantly and reversibly increased channel activity both for α_{1B} alone (2.4-fold increase) and for the α_{1B}/α_2-δ/β_{1b} combination (1.7-fold increase; see Fig. 12 for statistical details). The magnitude of these stretch-induced activity increases were comparable to the ~1.5-fold stretch-induced peak I_{Ba} increases measured in the macroscopic current experiments. Inspection of both the overlapped traces and the all-points histograms shows there are no grounds for suggesting that stretch increased the amplitude of the fully open state. Because subconductance events were characteristic of

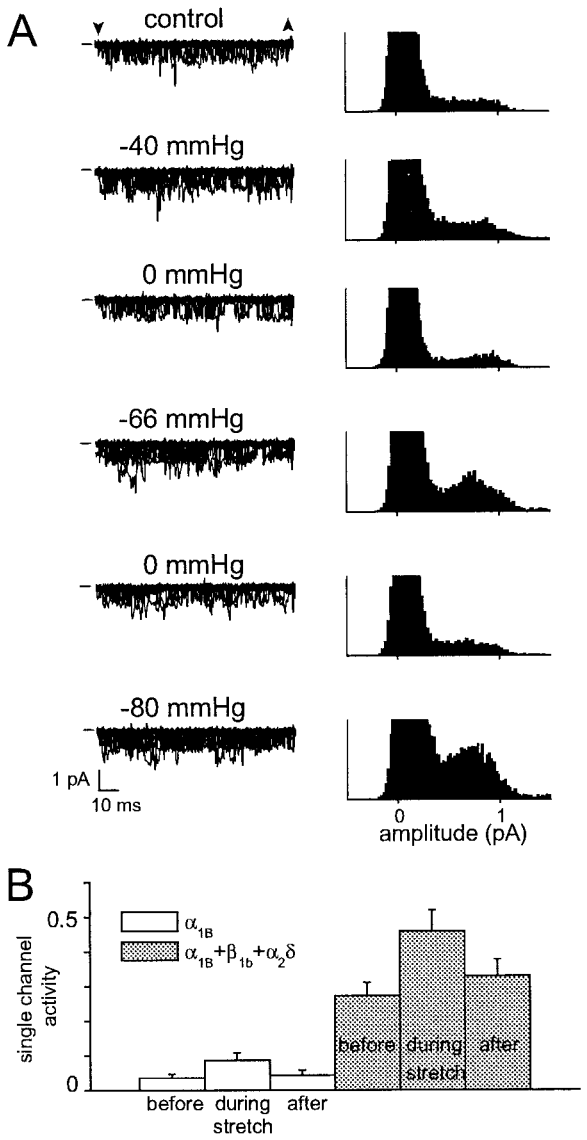

FIGURE 12 Single-channel recordings from cells transfected with $\alpha_{1B}/\alpha_2\text{-}\delta/\beta_{1b}$. (*A*) On the left are current records (20 overlapped episodes/condition) elicited by steps to 20 mV from −70mV. On the right are all-points histograms (bin-width, 0.021 pA). (*B*) Single-channel activity (as defined in Materials and Methods) as a fraction of the total recording time before, during, and after stretch. The corresponding values for patches from cells transfected with only α_{1B} were 0.036 ± 0.011, 0.086 ± 0.023, and 0.042 ± 0.015 (*white bars*; $n = 8$ applications of suction −8/−60 mm Hg; $n = 6$ patches; paired *t*-test: $p < 0.03$ before/during stretch; $p < 0.006$ during/after stretch). For cells transfected with the $\alpha_{1B}/\alpha_2\text{-}\delta/\beta_{1b}$ combination they were 0.27 ± 0.040, 0.46 ± 0.015, and 0.32 ± 0.048 (*gray bars*; $n = 12$ applications of suction −14/−80 mm Hg; $n = 6$ patches; paired *t*-test: $p < 0.0009$ before/during stretch; $p < 0.019$ during/after stretch)

control records for both α_{1B} alone and for the $\alpha_{1B}/\alpha_2\text{-}\delta/\beta_{1b}$ combination, a possible explanation for the stretch-induced increase of N-type current was that stretch transformed subconductance events into full-conductance events. Although the brevity and amplitude spread of the subconductance levels prevented their precise quantitation, the histograms argue against the possibility of stretch-induced conductance level switch; the sub- and full-conductance contributions to histograms increased about equally during stretch.

Thus, the single-channel data demonstrated the following: 1) α_{1B} subunits alone can generate mechanosensitive N-type channels, and 2) unitary current amplitude is not mechanosensitive. By elimination, mechanosensitivity probably resides with channel kinetics and/or the number of functional channels. Given the presence of subconductances, the small amplitude and short duration of the unitary current events, and the lack of a striking qualitative stretch effect (e.g., a switch from sub- to full-conductance), however, extensive data sets will be required to uncover any stretch-sensitive effects on N or P_o. Additional investigations might most profitably be done with channel variants that tend to make more prolonged openings.

Action potential clamp recordings and stretch

Finally, we wished to gauge whether the mechano-responses of N-type currents would be perceptible during the sorts of brief repetitive voltage excursions experienced in neurons. We performed AP clamp recordings under whole-cell clamp (see Materials and Methods), applying a series of nine AP trains (frequency, one train per 20 s). Within each train, the peak AP amplitude fell with time, giving a ratio of the ninth to the first of 0.8 ± 0.04 ($n = 4$) that was insensitive to stretch (data not shown). In Fig. 13 *A*, the peak value of the first AP of each train is plotted as a function of time (i.e., at 20-s intervals). Every time positive pressure inflated the cell, increase peak I_{Ba} increased (by 26 ± 3%; $n = 6$, from 4 cells). This ~1.3-fold increase in the magnitude of N-type current during spike trains is consistent with what was observed for steps. Insofar as the inward currents attained their prestretch levels faster during the APs, a nontrivial consequence of stretch-augmented currents in vivo could be to accelerate as well as increase intracellular $[Ca^{2+}]$ changes during spikes. AP waveform trains applied to nontransfected cells (Fig. 13 *B*, *left*) elicited no inward current, and cell inflation had no effect on the recorded current in these cells (Fig. 13 *B*, *right*).

DISCUSSION

Overview

For recombinant N-type channels in a cell line, we observed a phenomenon seen in many native preparations for L-type currents (references in Introduction): membrane stretch increases the peak current ~1.5-fold. Despite the potential physiological and/or pathological interest of mechanosensitive calcium currents, the reports from smooth muscle cells have attracted little attention (e.g., Catterall, 2000; Jaggar et al., 2000). Perhaps there have been concerns that the responses depend as much on the recording conditions as on

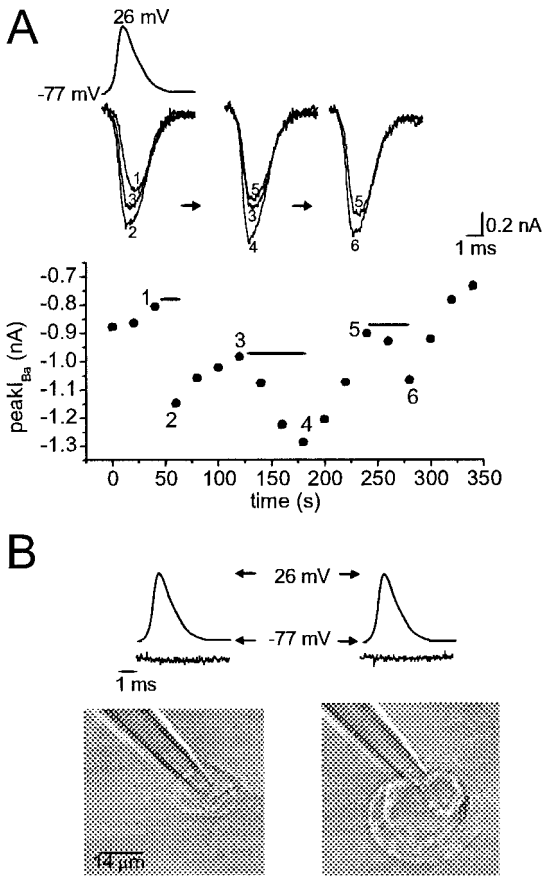

FIGURE 13 Stretch during AP-like voltage excursions. (*A*) At a frequency of one train per 20 s, trains of 9 AP excursions from −77 mV to +26 mV and back, as shown, were applied at 1 or 10 Hz. Current traces elicited by AP waveforms were selected (as indicated by the numbers) from the peak I_{Ba} time course plotted below. Filled bars indicate when positive pressure was applied. (*B*) Current traces elicited by the same AP waveforms in a nontransfected cell without (*left*) and with (*right*) pressure.

the channels themselves. We found, however, that a T-type channel construct did not respond to stretch, even when coexpressed and costimulated with N-type channels. This strongly suggests that either the channels themselves or their subtype-specific arrangements in the plasma membrane underlie the susceptibility of the N-type currents to membrane stretch. Unpublished preliminary results for recombinant L-type channels (B. Calabrese and C. E. Morris) in HEK cells confirmed the stretch-induced increase reported from native cells. Mechano-responses shared by native L-type and recombinant N-type (and L-type) calcium channels are presumably not reliant on native cell morphological and biochemical specializations. In addition to the stretch-induced peak current increase, N-type channels showed several other effects, some reversible (e.g., enhanced rate of inactivation from open states) and some not (e.g., enhanced rate of inactivation from closed states). The irreversible effects were like stretch accelerations of spontaneous run-down processes and as such may have links to what in intact cells would be classed as modulation (e.g., Kepplinger et al., 2000).

Membrane tension and voltage-gated channels

Stretch effects on N-type channels are very unlike effects on a simpler voltage-gated channel, Shaker. In Shaker, reversible stretch activation (Gu et al., 2001) depends on increased activation rates that produce a hyperpolarizing shift of the $G(V)$ and no change in G_{max} (Tabarean and Morris, 2002). By contrast, for N-type calcium channels, stretch increased G_{max} but did not shift $G(V)$ or alter the rate of activation. Because we reliably detected small changes in the rate of N-type activation during run-up, temporal resolution was not an obvious problem. In calcium channels, as in Shaker and sodium channels, gating charge movements are tightly coupled to pore opening (Olcese et al., 1996); accordingly, if stretch facilitates gating charge movements, one might expect all these voltage-gated channels to make qualitatively similar changes in activation during stretch. The picture that is emerging is, however, more complex than that. Voltage-gated sodium and potassium channels in squid under hyperbaric conditions (Conti et al., 1984) and Shaker channels in oocytes (Meyer and Heinemann, 1997) activate faster at atmospheric pressure than when compressed, as if the channels expand during voltage activation. Expansion in the plane of the bilayer would be consistent with the responses of recombinant Shaker to stretch (Tabarean and Morris, 2002). Nothing, however, in the responses of N-type channels suggests that they expand during voltage gating. The conundrum is deepened by the fact that in a mammalian sodium channel (α-subunit only), activation rates are not reversibly stretch sensitive even though stretch can irreversibly affect other aspects of the channel's behavior, making the anomalously slow-gating α-subunit gate in the way it normally does with the β-subunit present (Tabarean et al., 1999). Likewise, we found that stretch that irreversibly changed inactivation of N-type currents (whole-cell conditions) had no impact on activation rates. Thus, whatever is signified by the reversible mechano-responses of Shaker and of squid channels, we have to conclude that in neither N- nor T-type calcium channels (nor skeletal muscle sodium channels) do the voltage sensors feel membrane tension in any appreciable way.

We can rule out the possibility that auxiliary subunits somehow prevented the calcium channels from responding to stretch like Shaker, first, because T-type currents arising from an α_{1I} subunit alone showed no stretch-sensitive activation and, second, because N-type currents through α_{1B} subunits were stretch sensitive with or without the auxiliary subunits. The mechanosensitivity of N-type current thus differs qualitatively from that of the inherently mechano-susceptible homotetrameric membrane protein Shaker. Finally, we emphasize that our results for the T-type channel

were for one construct and should not be used to assert that all T-type channels are insensitive to stretch.

The mechano-responses of N- and L-type calcium channels bear little overall resemblance to those of bacterial osmotic-valve stretch channels (Sukharev et al., 2001), where elevated membrane tension alone (albeit at near-lytic levels) can change P_o from zero to near unity, or to the two-pore domain K^+ channels of excitable cells (Patel et al., 2001), for which the same is true at somewhat lower tensions. These K^+ channels would broadly coexist in central neurons with N-type calcium channels. Evidence that they perform physiological mechano-tasks has not been forthcoming, but in vitro, we note, they respond to the same range of mechanical stimuli shown here to act on N-type calcium channels.

Stretch and increased G_{max} for N-type channels.

Stretch transiently increased G_{max} for N-type channels, and the effect could be elicited repeatedly. The apparent increase in the number of channels was not caused by membrane addition because even when cells inflated twofold, their plasma membrane area remained fixed. Inflation-induced smoothing of excess surface area (Solsona et al., 1998; Raucher and Sheetz, 1999) inevitably involves disruption of long-range plasma membrane structure. How, at fixed membrane area, stretch might abruptly yet transiently (seconds, not minutes or hours) increase the density of functional N-type (but not coexpressed T-type) channels is difficult to fathom. Because some channels traffic to the surface in mechanically specialized domains (Martens et al., 2001), one possibility is that a subpopulation of channels sequestered in lipid rafts is reversibly recruited during stretch to the pool of operating channels. Such a scenario is envisaged for c-Src tyrosine kinase inhibition of volume-regulated anion channels, which seems to require compartmentalization of the kinase to membrane subdomains (Trouet et al., 2001).

Another possibility is stretch reactivation of channels lost to run-down. Mechanisms suggested for Ca^{2+} channel run-down include proteolysis (Romanin et al., 1991), dephosphorylation (Ono and Fozzard, 1992; Costantin et al., 1999), and washout of the cytoplasmic factor calpastatin (Kameyama et al., 1998), which evidently can target calcium channel subunits (Kepplinger et al., 2000). Because stretch-induced I_{peak} sometimes exceeded initial values (e.g., Fig. 3 *A*), invoking a reactivation mechanism would imply that at the time of whole-cell access, some channels were in a down-modulated state. The fact that cell-attached patches (where run-down is not a factor) show the stretch-induced increase in peak current, however, tends to undermine the stretch reactivation idea.

Single-channel recordings of calcium currents before, during, and after stretch showed that NP_o increased reversibly with stretch, with no obvious change in the single-channel current amplitude. This suggests that the change may be kinetic, but our data did not let us rule out the possibility that stretch transiently increases N (the number of operational channels) as the macroscopic currents seem to suggest. This idea is testable at the single-channel level, but long-lasting unitary events from BAYK 8644-treated L-type channels or an N-type mutant that makes prolonged openings will be needed.

Mechanical stimulus

Pressures applied under whole-cell clamp ranged from 2 to 15 mmHg (i.e., 267-2000 N/m^2), which, assuming spherical geometry and applying Laplace's Law ($T = Pr/2$) would correspond to membrane tensions of 2–9 mN/m. For most biological membranes, lytic tensions are ~10 mN/m (Morris and Homann, 2001). Only in cells that visibly inflated with pressure either immediately or within tens of seconds did we obtain mechano-effects, but more precisely what this means in terms of mechanical changes at the plasma membrane we do not know. Stretch-I_{peak} increases correlated not with pressure but with the extent of cell inflation. They also coincided temporally with inflation. By contrast, stretch acceleration of inactivation began as soon as pressure was applied, even when detectable inflation did not occur until many seconds later (e.g., Figs. 3 *B* and 7 *A*). This suggests that distinct mechanical perturbations underlie effects on peak current and on inactivation kinetics. Plasma membrane is not a classic Hookean solid; concepts of stress (reversible extension) and strain (irreversible extension) in response to applied force are not rigorously applicable. Membrane-associated structures at various size scales (e.g., individual membrane proteins, lipid rafts, and membrane skeleton) will respond in many fashions to the same applied pressure and healing, or mechanical memory, may be a factor. Consider several possibilities: stretch-disruption of long- or short-range membrane skeleton complexes (Lee and Discher, 2001), stretch flattening of caveolae (Dulhunty and Franzini-Armstrong, 1975), stretch regulation of a membrane kinase (Kimura et al., 2000), stretch dissociation of heteromeric channel subunits, and stretch alteration of the membrane ceramide content (Chik et al., 1999). Each could be reversible or irreversible, depending on the state of the cytoplasm.

The reversibility of stretch-induced increase in I_{peak} was difficult to evaluate in whole-cell recordings not only because of run-down but also because deflation after a positive pressure pulse could be slow. However, the reversibility of this phenomenon was confirmed in cell-attached recordings where application and release of membrane tension is more straightforward.

Before leaving the topic of our mechanical stimuli, we should discuss the possibility of unintended cell swelling. Cell swelling immediately after whole-cell access was suggested by Langton (1993) as a way to explain run-up. That can be excluded here because 1) in our experiments detectable cell swelling after whole-cell access was rare, whereas the run-up was invariably present (unless high-speed puls-

ing was used); 2) if, for a minute or so after going whole-cell (i.e., beyond the usual run-up time) the membrane was left unclamped (and hence rather depolarized) before applying the standard protocol (−90 mV with 5-s inter-episodes), a run-up of I_{peak} was still obtained; and 3) high-frequency protocols applied right from the outset prevented run-up. We think therefore that run-up reflected a slowly recovering gating mode in the N-type Ca^{2+} channels and was not a cryptic stretch effect caused by post-access swelling.

Do effects of stretch on inactivation cancel the effect on activation?

Unlike classic Na^+ or K^+ channel inactivation, N-type Ca^{2+} channel inactivation shows almost no voltage overlap with steady-state activation, so during trains of brief pulses, inactivation occurs predominantly from intermediate closed states (Patil et al., 1998). We found that stretch significantly enhanced this process. Additionally, stretch transiently accelerated inactivation from the open state, exacerbating a process occurring spontaneously with time under whole-cell conditions. Finally, stretch irreversibly left-shifted inactivation (Fig. 6, *B* and *C*), again exacerbating or amplifying a spontaneous process. If these effects of stretch on inactivation were to occur in vivo would they overwhelm the stretch-induced increase in N-type current? We conclude that they probably would not from our finding that during voltage clamp excursions mimicking repeated bursts of action potentials, stretch accelerated the development of the calcium current and increased its overall magnitude at the AP peaks. Cell-attached experiments suggested that with intact cytoplasm, stretch would have little impact on the rate of inactivation, and this might mean that stretch impacts on net calcium entry could be appreciably greater than seen in whole-cell recordings. The stretch-induced left-shift of inactivation that we report (whole-cell) developed progressively, however, so it may be that for cells subjected to prolonged mechanical trauma (e.g., Agrawal et al., 2000), a progressive left-shift of inactivation could counteract calcium loading via the channels. Hyperbaric depression of synaptic transmission is specifically dependent on suppression of synaptic N-type calcium channel activity (Etzion and Grossman, 2000); perhaps the complex mechanosensitivity of N-type channels contributes to this pressure phenomenon.

In immature neurons, where N-type calcium channels are a prerequisite for directed migration (Komuro and Rakic, 1992), growth cone membrane tension might be high due to traction forces (Lamoureux et al., 1998). Of particular interest are the L- and N-type channels located near load-bearing focal adhesions, which appear to regulate actin-myosin dynamics and the remodeling of the load-bearing membrane skeleton (Zimprich and Bolsover, 1996; Archer et al., 1999). It is intriguing to consider that when dendritic spines contract (Halpain, 2000), membrane tension would likely change not only in the postsynaptic membrane (as discussed by Korkotian and Segal, 2001) but also in the adherent presynaptic membrane. Although our results suggest that the modulation by stretch of N-type (and L-type) channels near mechanically active synapses and growth cones is a possibility, it will be an interesting challenge to determine whether such channels in situ mediate stretch-induced increases in calcium influx.

NOTE ADDED IN PROOF

A recombinant L-type α-subunit cloned from human smooth muscle has also just been reported to be mechanosensitive (Lyford et al., 2001)

We are grateful to Dr. Steve Barnes for comments on the manuscript and to Dr. Petro Doroshenko for use of the frame grabber.

This work was supported by operating grants to C.E.M. from the Canadian Institutes of Health Research, NSERC (Natural Sciences and Engineering Research Council) Canada, and the Hearth and Stroke Foundation of Ontario (T3461).

REFERENCES

Agrawal, S. K., R. Nashmi, and M. G. Fehlings. 2000. Role of L- and N-type calcium channels in the pathophysiology of traumatic spinal cord white matter injury. *Neuroscience.* 99:179–188.

Archer, F. R., P. Doherty, D. Collins, and S. R. Bolsover. 1999. CAMs and FGF cause a local submembrane calcium signal promoting axon outgrowth without a rise in bulk calcium concentration. *Eur. J. Neurosci.* 11:3565–3573.

Borst, J. G. G., F. Helmchen, and B. Sakmann. 1995. Pre- and postsynaptic whole-cell recordings in the medial nucleus of the trapezoid body of the rat. *J. Physiol. (Lond.).* 489:825–840.

Catterall, W. A. 2000. Structure and regulation of voltage-gated Ca^{2+} channels. *Annu. Rev. Cell. Dev. Biol.* 16:521–555.

Chik, C. L., B. Li, T. Negishi, E. Karpinski, and A. K. Ho. 1999. Ceramide inhibits L-type calcium channel currents in rat pinealocytes. *Endocrinology.* 140:5682–5690.

Churchwell, K. B., S. H. Wright, F. Emma, P. A. Rosenberg, and K. Strange. 1996. NMDA receptor activation inhibits neuronal volume regulation after swelling induced by veratridine-stimulated Na^+ influx in rat cortical cultures. *J. Neurosci.* 16:7447–7457.

Conti, F., I. Inoue, F. Kukita, and W. Stühmer. 1984. Pressure dependence of sodium gating currents in the squid giant axon. *Eur. Biophys. J.* 11:137–147.

Costantin, J. L., N. Qin, M. N. Waxham, L. Birnbaumer, and E. Stefani. 1999. Complete reversal of run-down in rabbit cardiac Ca^{2+} channels by patch-cramming in *Xenopus* oocytes: partial reversal by protein kinase A. *Pflügers Arch.* 437:888–894.

Dulhunty, A. F., and C. Franzini-Armstrong. 1975. The relative contributions of the folds and caveolae to the surface membrane of frog skeletal muscle fibres at different sarcomere lengths. *J. Physiol.* 250:513–539.

Etzion, Y., and Y. Grossman, 2000. Pressure-induced depression of synaptic transmission in the cerebellar parallel fibre synapse involves suppression of presynaptic N-type Ca^{2+} channels. *Eur. J. Neurosci.* 12: 4007–4016.

Gu, C. X., P. F. Juranka, and C. E. Morris. 2001. Stretch-activation and stretch-inactivation of Shaker-IR, a voltage-gated K^+ channel. *Biophys. J.* 80:2678–2693.

Halpain, S. 2000. Actin and the agile spine: how and why do dendritic spines dance? *Trends Neurosci.* 23:141–146.

Hamill, O. P., and B. Martinac. 2001. Molecular basis of mechanotransduction in living cells. *Physiol. Rev.* 81:685–740.

Hamill, O. P., A. Marty, E. Neher, B. Sakmann, and F. J. Sigworth. 1981. Improved patch-clamp techniques for high-resolution current recording from cells and cell-free membrane patches. *Pflügers Arch.* 391:85–100.

Holm, A. N., A. Rich, M. G. Sarr, and G. Farrugia. 2000. Whole cell current and membrane potential regulation by a human smooth muscle mechanosensitive calcium channel. *Am. J. Physiol. Gastrointest. Liver Physiol.* 279:G1155–G1161.

Jaggar, J. H., V. A. Porter, W. J. Lederer, and M. T. Nelson. 2000. Calcium sparks in smooth muscle. *Am. J. Physiol. Cell Physiol.* 278:C235–C256.

Jones, L. P., C. D. DeMaria, and D. T. Yue. 1999. N-type calcium channel inactivation probed by gating-current analysis. *Biophys. J.* 76: 2530–2552.

Kameyama, M., A. Kameyama, E. Takano, and M. Maki. 1998. Run-down of the cardiac L-type Ca^{2+} channel: partial restoration of channel activity in cell-free patches by calpastatin. *Pflügers Arch.* 435:344–349.

Kepplinger, K. J. F., G. Förstner, H. Kahr, K. Leitner, P. Pammer, K. Groschner, N. M. Soldatov, and C. Romanin. 2000. Molecular determinants for run-down of L-type Ca^{2+} channels localized in the carboxyl terminus of the α_{1C} subunit. *J. Physiol.* 529:119–130.

Kimura, M., K. Obara, T. Sasase, T. Ishikawa, Y. Tanabe, and K. Nakayama. 2000. Specific inhibition of stretch-induced increase in L-type calcium channel currents by herbimycin A in canine basilar arterial myocytes. *Br. J. Pharmacol.* 130:923–931.

Korkotian, E., and M. Segal. 2001. Spike-associated fast contraction of dendritic spines in cultured hippocampal neurons. *Neuron.* 30:751–758.

Komuro, H., and P. Rakic. 1992. Selective role of N-type calcium channels in neuronal migration. *Science.* 257:806–809.

Lamoureux, P., R. E. Buxbaum, and S. R. Heidemann. 1998. Axonal outgrowth of cultured neurons is not limited by growth cone competition. *J. Cell Sci.* 111:3245–3252.

Langton, P. D. 1993. Calcium channel currents recorded from isolated myocytes of rat basilar artery are stretch sensitive. *J. Physiol.* 471:1–11.

Lee, J. H., A. N. Daud, L. L. Cribbs, A. E. Lacerda, A. Pereverzev, U. Klockner, T. Schneider, and E. Perez-Reyes. 1999. Cloning and expression of a novel member of the low voltage-activated T-type calcium channel family. *J. Neurosci.* 19:1912–1921.

Lee, J. C., and D. E. Discher. 2001. Deformation-enhanced fluctuations in the red cell skeleton with theoretical relations to elasticity, connectivity, and spectrin unfolding. *Biophys. J.* 81:3178–3192.

Lyford, G. L., P. R. Strege, A. Shepard, Y. Ou, L. Ermilov, S. M. Miller, S. J. Gibbons, J. L. Rae, J. H. Szurszewski, and G. Farrugia. 2002. α(1C)(Ca(V)1.2) L-type calcium channel mediates mechanosensitive calcium regulation. *Am. J. Physiol. Cell Physiol.* 283:C1001–C1008.

Martens, J. R., N. Sakamoto, S. A. Sullivan, T. D. Grobaski, and M. M. Tamkun. 2001. Isoform-specific localization of voltage-gated K^+ channels to distinct lipid raft populations: targeting of Kv1.5 to caveolae. *J. Biol. Chem.* 276:8409–8414.

Matsuda, N., N. Hagiwara, M. Shoda, H. Kasanuki, and S. Hosoda. 1996. Enhancement of the L-type Ca^{2+} current by mechanical stimulation in single rabbit cardiac myocytes. *Circ. Res.* 78:650–659.

Matzner, O., S. Ben-Tabou, and I. Nussinovitch. 1996. Hyperosmotic regulation of voltage-gated calcium currents in rat anterior pituitary cells. *J. Neurophysiol.* 75:1894–1900.

Meir, A., and A. C. Dolphin. 1998. Known calcium channel α1 subunits can form low threshold small conductance channels with similarities to native T-type channels. *Neuron.* 20:341–351.

Meyer. R., and S. H. Heinemann. 1997. Temperature and pressure dependence of Shaker K^+ channel N- and C-type inactivation. *Eur. Biophys. J.* 26:433–445.

Moreno Davila, H. 1999. Molecular and functional diversity of voltage-gated calcium channels. *Ann. N.Y. Acad. Sci.* 868:102–117.

Morris, C. E., and U. Homann. 2001. Cell surface area regulation and membrane tension. *J. Membr. Biol.* 179:79–102.

Olcese, R., A. Neely, N. Qin, X. Wei, L. Birnbaumer, and E. Stefani. 1996. Coupling between charge movement and pore opening in vertebrate neuronal α_{1E} calcium channels. *J. Physiol.* 497:675–686.

Ono, K., and H. A. Fozzard. 1992. Phosphorylation restores activity of L-type Ca^{2+} channels after rundown in inside-out patches from rabbit cardiac cells. *J. Physiol.* 454:673–688.

Pappone, P. A., and S. C. Lee. 1996. Purinergic receptor stimulation increases membrane trafficking in brown adipocytes. *J. Gen. Physiol.* 108:393–404.

Patel, A. J., M. Lazdunski, and E. Honore. 2001. Lipid and mechano-gated 2P domain K(+) channels. *Curr. Opin. Cell. Biol.* 13:422–428.

Patil, P. G., D. L. Brody, and D. T. Yue. 1998. Preferential closed-state inactivation of neuronal calcium channels. *Neuron.* 20:1027–1038.

Raucher, D., and M. P. Sheetz. 1999. Characteristics of a membrane reservoir buffering membrane tension. *Biophys. J.* 77:1992–2002.

Romanin, C., P. Grösswagen, and H. Schindler. 1991. Calpastatin and nucleotides stabilize cardiac Ca^{2+} channel activity in excised patches. *Pflügers Arch.* 418:86–92.

Ruiz-Velasco, V., M. B. Mayer, and L. J. Hymel. 1996. Dihydropyridine-sensitive Ca^{2+} influx modulated by stretch in A7r5 vascular smooth muscle cells. *Eur. J. Pharmacol.* 296:327–334.

Ryder, K. D., and R. L. Duncan. 2001. Parathyroid hormone enhances fluid shear-induced $[Ca^{2+}]_i$ signaling in osteoblastic cells through activation of mechanosensitive and voltage-sensitive Ca^{2+} channels. *J. Bone Miner. Res.* 16:240–248.

Small, D. L., and C. E. Morris. 1994. Delayed activation of single mechanosensitive channels in *Lymnaea* neurons. *Am. J. Physiol.* 267: C598–C606.

Solsona, C., B. Innocenti, and J. M. Fernandez. 1998. Regulation of exocytotic fusion by cell inflation. *Biophys. J.* 74:1061–1073.

Sukharev, S., M. Betansos, C-S. Chiang, and H. R. Guy. 2001. The gating mechanism of the large mechanosensitive channel MscL. *Nature.* 409: 720–724.

Tabarean, I. V., P. Juranka, and C. E. Morris. 1999. Membrane stretch affects gating modes of a skeletal muscle sodium channel. *Biophys. J.* 77:758–774.

Tabarean, I. V., and C. E. Morris. 2002. Membrane stretch accelerates activation and slow inactivation in Shaker channels with S3–S4 deletions. *Biophys. J.* 82:2982–2994.

Trouet, D., I. Carton, D. Hermans, G. Droogmans, B. Nilius, and J. Eggermont. 2001. Inhibition of VRAC by c-Src tyrosine kinase targeted to caveolae is mediated by the Src homology domains. *Am. J. Physiol. Cell Physiol.* 281:C248–C256.

Xu, W. X., S. J. Kim, S. J. Kim, I. So, T. M. Kang, J. C. Rhee, and K. W. Kim. 1996. Effect of stretch on calcium channel currents recorded from the atrial circular myocytes of guinea-pig stomach. *Pflügers Arch.* 432: 159–164.

Zimprich, F., and S. R. Bolsover. 1996. Calcium channels in neuroblastoma cell growth cones. *Eur. J. Neurosci.* 8:467–475.